Supplementary Information for Chaturbedi and Lee

Different gametogenesis states uniquely impact longevity in *Caenorhabditis elegans*.

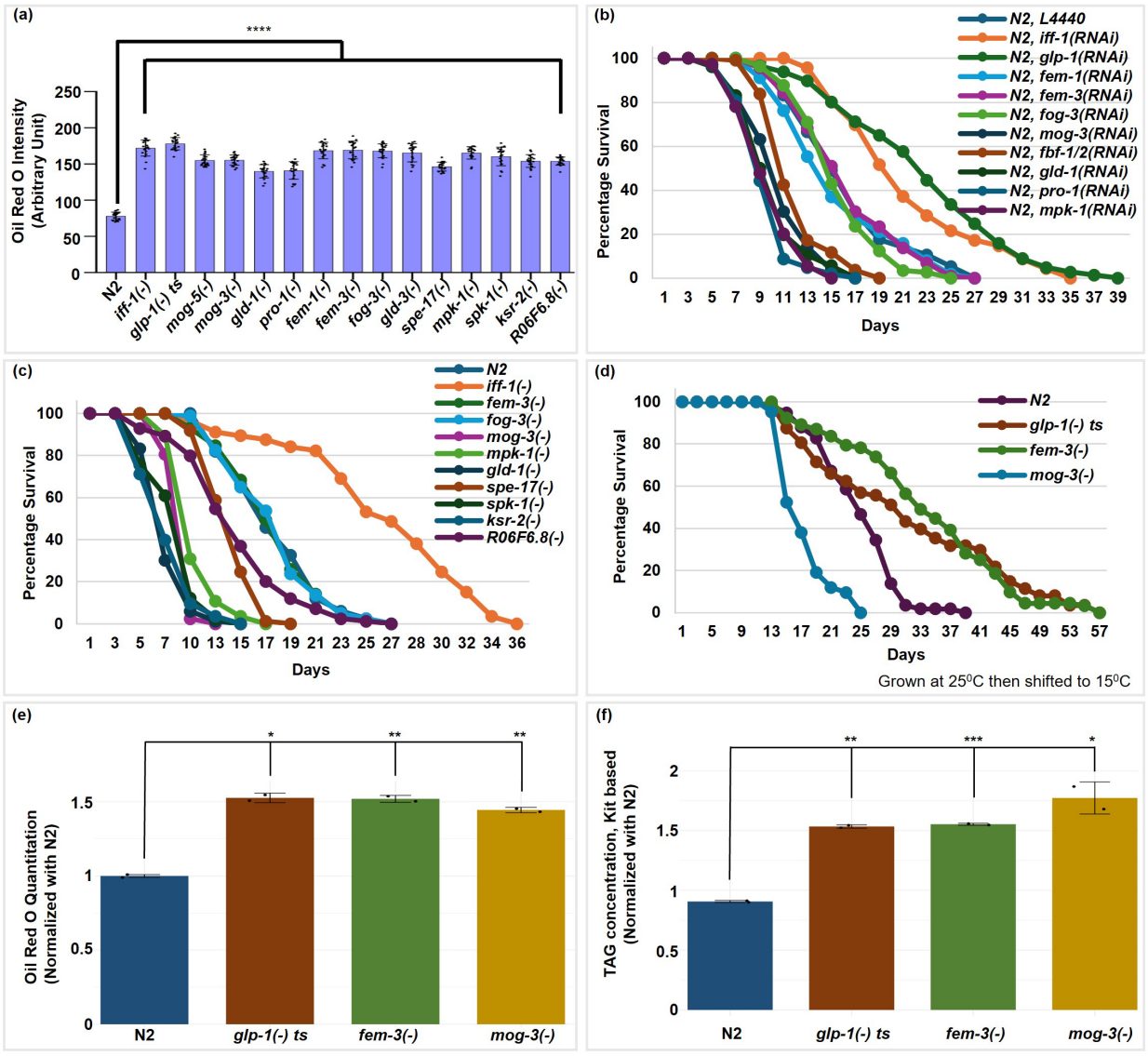

Supplementary Fig. 1: Sterile strains displayed excessive lipid accumulation but different lifespans. (a) Oil red O (ORO) intensity in the indicated sterile strains (day 1 adults). All three sterile mutants accumulated excess fat. ORO intensity was shown as the mean of two biological replicates per genotype, with at least 10 worms per replicate and 20 worms total per genotype. In panel a, the p-values for comparisons with N2 ranged from 5.6×10^{-34} to 4.9×10^{-24}. (b, c, d) Survival curves showing the lifespans (at 20°C) of wild-type worms treated with the indicated gene RNAi (b), the lifespans (at 20°C) of wild-type and mutant strains (c), the lifespans of wild-type N2, *glp-1(e2144)*, *fem-3(e1996)* and *mog-3(q74)* worms grown at 25°C then aged at 15°C (d). In panels b, c, and d, two biological replicates were analyzed for each genotype. Detailed mean lifespan values, the number of worms analyzed per replicate, and corresponding statistical analyses are provided in Source Data. (e, f) Lipid levels in wild-type N2, *glp-1(e2144)*, *fem-3(e1996)* and *mog-3(q74)* worms (day 1 adults) based on the optical density of extracted Oil Red O from 100 worms (e), and calorimetry-based triacylglycerides (TAG) kit (normalized with N2) (f). ORO (e) and TAG (f) levels were quantified from lysates prepared from approximately 100

worms per replicate, with two biological replicates performed for each assay. In panel e, the p-values for comparisons with N2 are 0.0181 for *glp-1(-) ts*; 0.0082 for *fem-3(-)*, and 0.0049 for *mog-3(-)*, respectively. In panel f, the p-values for comparisons with N2 are 0.0014 for *glp-1(-) ts*; 0.00016 for *fem-3(-)*, and 0.0485 for *mog-3(-)*, respectively. In panels d, g and e unpaired two-tailed Welch's t-tests were used to perform one-way comparisons of each genotype to N2. No correction for multiple comparisons was applied. Statistical significance was set at $p < 0.05$. p-values for the tests are indicated as $*p < 0.05$, $**p < 0.01$ $***p < 0.001$. Error bars represent standard deviations.

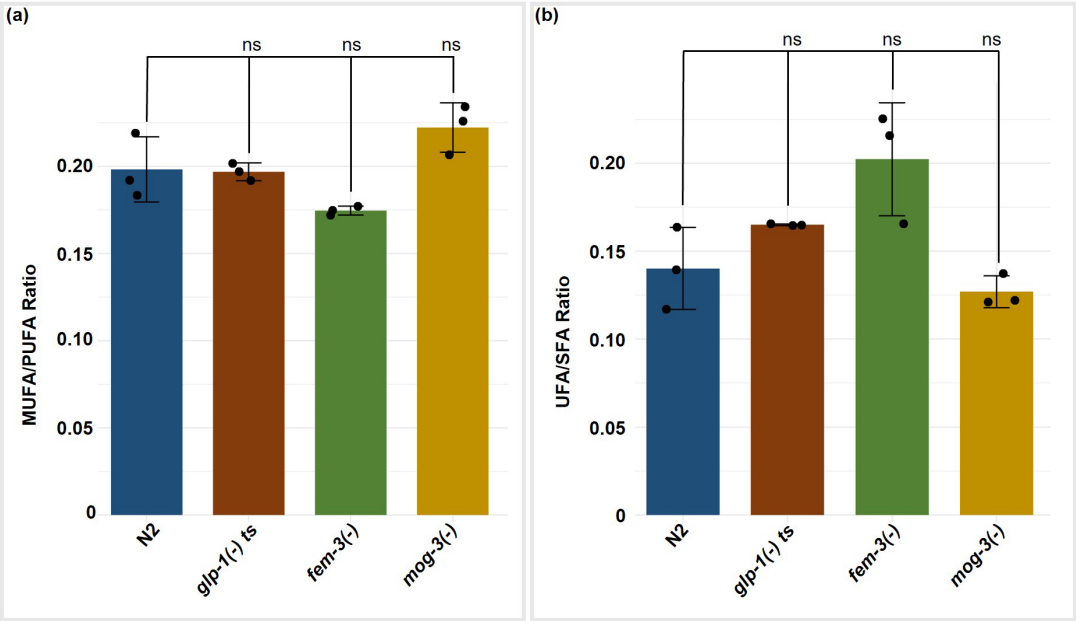

Supplementary Fig. 2: Sterile mutants exhibit similar lipid profiles. (a) The ratio of total monounsaturated fatty acids (MUFA) to polyunsaturated fatty acids (PUFA) in wild-type N2, *glp-1(e2144)*, *fem-3(e1996)*, and *mog-3(q74)*. While the ratios were higher in sterile mutants compared to wild-type, the increase did not reach statistical significance. In panel a, the p-values for comparisons with N2 are 0.9123 for *glp-1(-) ts*; 0.1579 for *fem-3(-)*, and 0.1567 for *mog-3(-)*, respectively. (b) The ratio of total UFA (unsaturated fatty acids) to SFA (saturated fatty acids) in wild-type *N2*, *glp-1(e2144)*, *fem-3(e1996)*, and *mog-3(q74)*. Ratios remained unchanged in the sterile mutants compared to wild-type. MUFA, PUFA and SFA estimations are based on three biological replicates from the lipidomics LC-MS dataset (see Methods for details). In panel b, the p-values for comparisons with N2 are 0.2055 for *glp-1(-) ts*; 0.0586 for *fem-3(-)*, and 0.4376 for *mog-3(-)*, respectively. In panels a and b unpaired two-tailed Welch's t-tests were used to perform one-way comparisons of each genotype to N2. No correction for multiple comparisons was applied. Statistical significance was set at $p < 0.05$. ns – not significant. Error bars represent standard deviations.

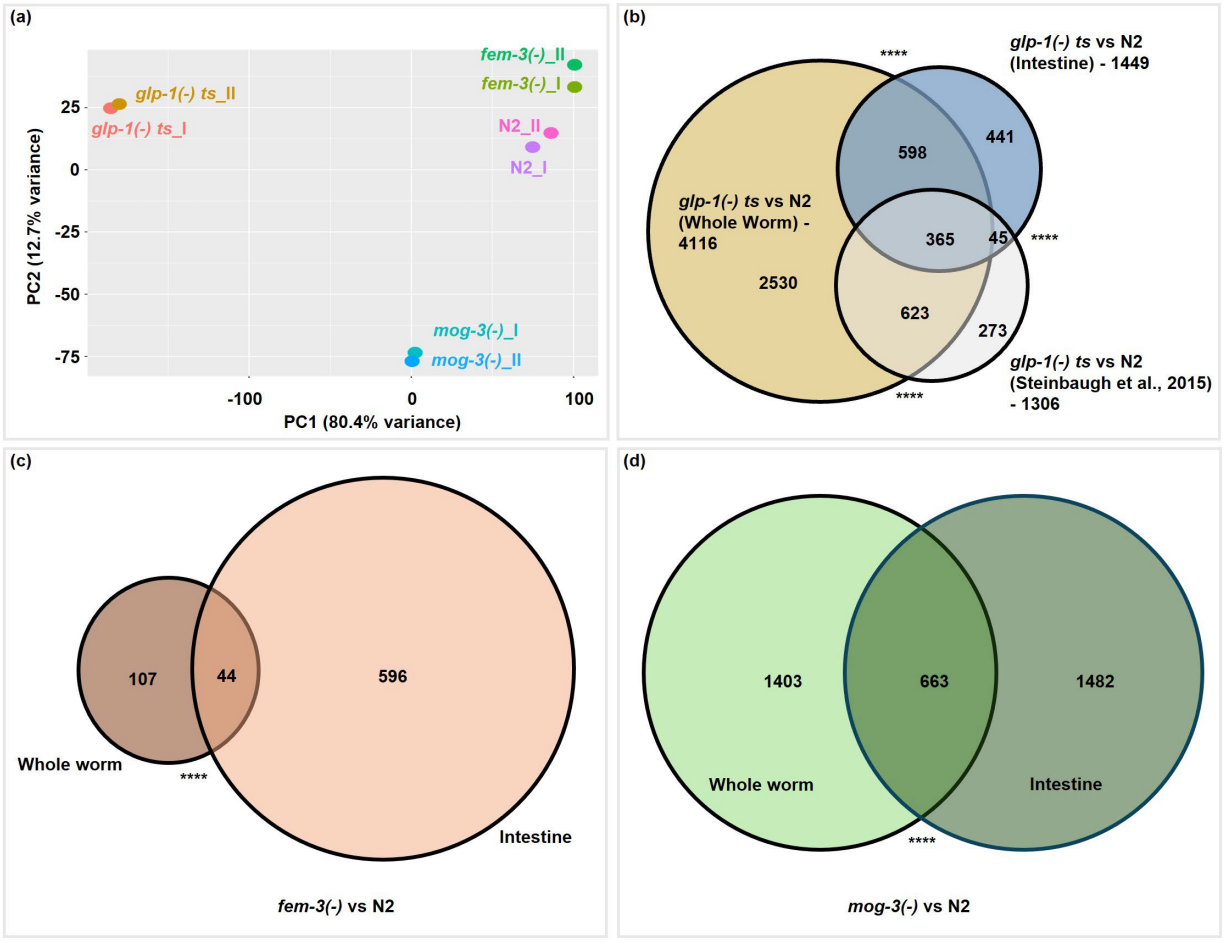

Supplementary Fig. 3: Whole-worm transcriptomic analysis of the sterile mutants.

(a) Principal components analysis (PCA) of the whole-worm RNA-seq data for two replicates of N2, *glp-1(e2144)*, *fem-3(e1996)* and *mog-3(q74)* worms. Each dot indicates one replicate. Long-lived *glp-1(e2144)* and *fem-3(e1996)* worms were clearly separated from short-lived *mog-3(q74)* worms on PC2. PCA plot was generated using R.(b) Venn diagram showed a significant overlap among the upregulated genes in *glp-1(e2144)* worms (relative to N2) in intestine-only, in whole-worm, and in a published data set[21]. The list of genes and overlaps are shown in Supplementary Data 2. (c, d) Venn diagrams showed the significant overlaps between the upregulated genes in *fem-3(e1996)* (c) (detailed list of genes shown in Supplementary Data 2) and *mog-3(q74)* (d) (detailed list of genes shown in Supplementary Data 2) relative to N2, in whole-worm and intestinal data sets. Fisher's exact test was used to assess the significance of overlaps in panel b, c and d. **** indicates p-value < 0.0001.

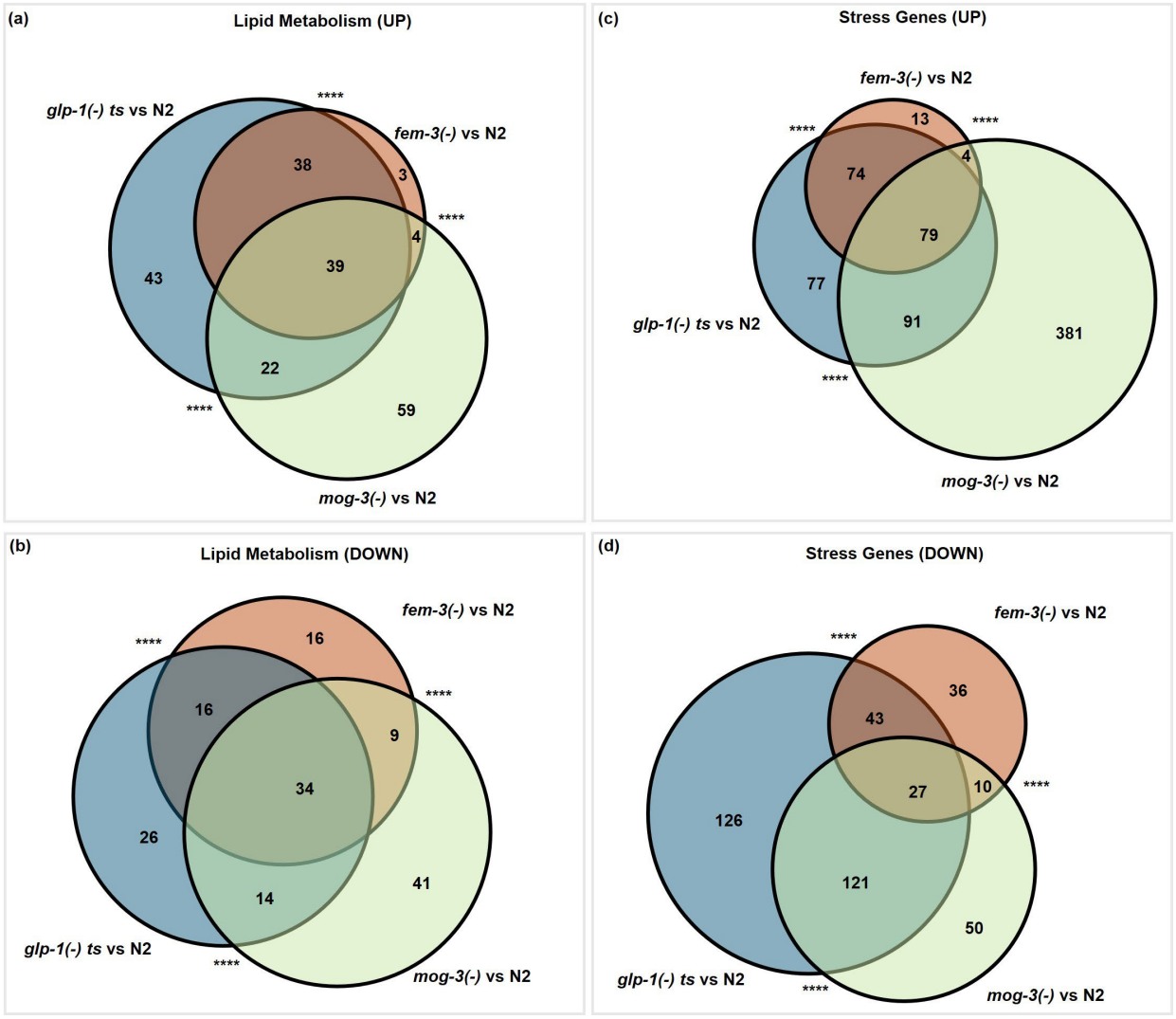

Supplementary Fig. 4: Lipid metabolism and stress response genes exhibit significant overlap among differentially regulated genes.

(a, b) Venn diagram showed the significant overlaps between the upregulated (UP) lipid metabolism genes (a) and stress response genes (b) in *glp-1(e2144), fem-3(e1996)* and *mog-3(q74)*, relative to N2. The gene lists and overlaps in lipid metabolism genes and stress response genes are shown in Supplementary Data 2. (c, d) Venn diagram showed the significant overlaps between the downregulated (DOWN) lipid metabolism genes (c) and stress response genes (d) in *glp-1(e2144), fem-3(e1996)* and *mog-3(q74)*, relative to N2. The gene lists and overlaps in lipid metabolism genes and stress response genes are shown in Supplementary Data 2. Fisher's exact test was used to assess the significance of overlaps in panel a, b, c and d. **** indicates p-value < 0.0001.

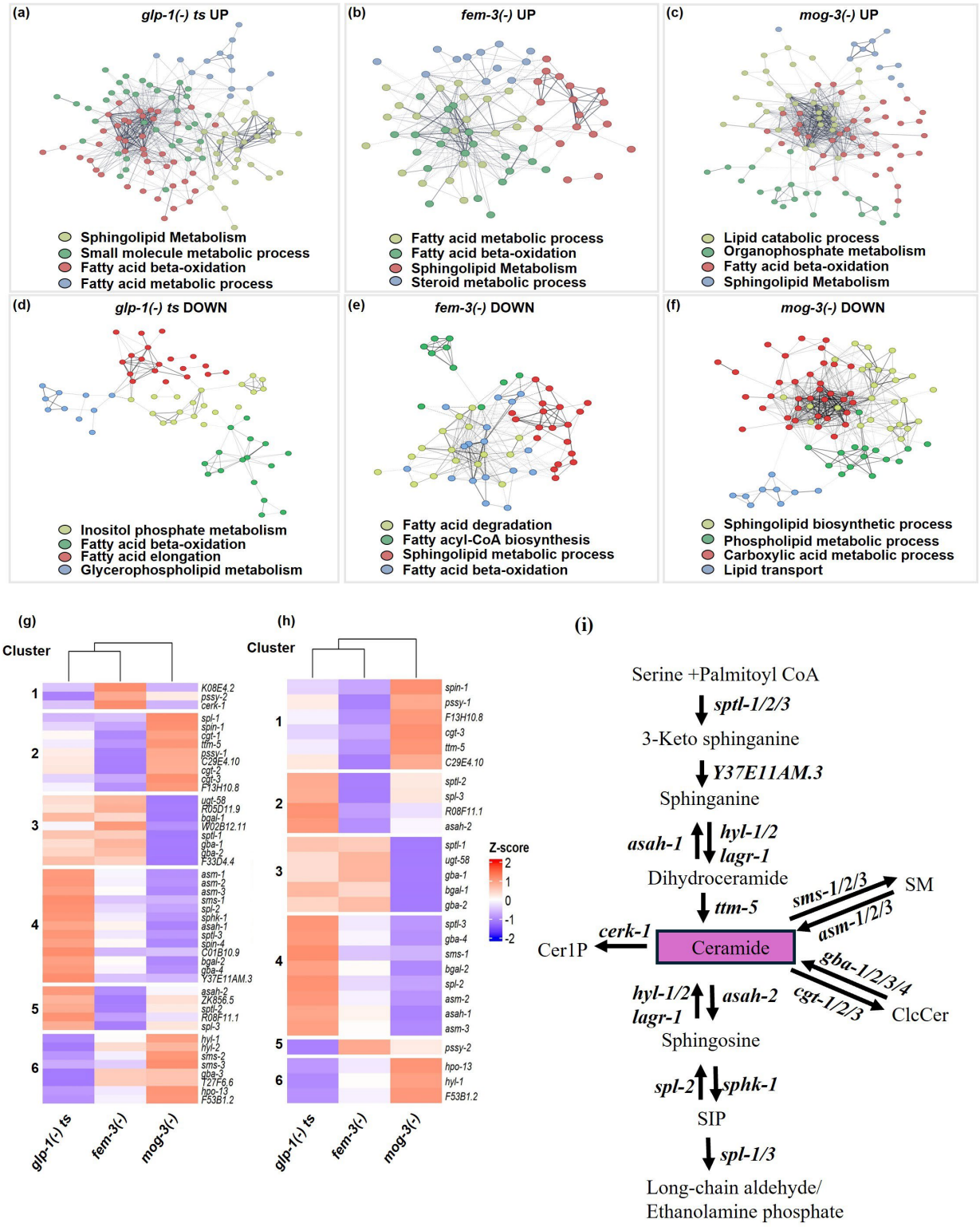

Supplementary Fig. 5: STRING analysis of differentially expressed lipid metabolism genes. (a–f) and heatmap of sphingolipid metabolism gene expression (log_2 fold change) in sterile mutants (g, h). (a, b, c)

K-means clustering showing the subgrouping of the upregulated fat metabolism genes in *glp-1(e2144)* (a), *fem-3(e1996)* (b) and *mog-3(q74)* (c) vs N2. The detailed list of genes in each cluster is shown in Supplementary Data 5. (d, e, f) K-means clustering showing the subgrouping of the downregulated fat metabolism genes in *glp-1(e2144)* (d), *fem-3(e1996)* (e) and *mog-3(q74)* (f) vs N2. The detailed list of genes in each cluster is shown in Supplementary Data 5. (g, h) Clustered heatmap of sphingolipid metabolism gene log2 fold change values relative to wild-type, derived from intestinal-specific RNA-seq data, shown both without any p-value cutoff (g) and with a 0.05 p-value cutoff (applied if significant in at least one genotype, h). The heatmap displays gene-wise (rows) clustering using K-means clustering (k = 6) and genotype-wise (columns) clustering using hierarchical clustering based on Pearson correlation distance and average linkage. Prior to clustering, log2 fold change values were z-score normalized across each gene to highlight relative expression differences. The clustering reveals that *glp-1(e2144)* and *fem-3(e1996)* mutants exhibit similar expression profiles, suggesting shared regulatory patterns, whereas *mog-3(q74)* clusters separately, reflecting its distinct transcriptional response. Color scale represents log2 fold change values relative to wild-type, with red indicating upregulation and blue indicating downregulation. The detailed lists of genes used to generate the heatmaps in panels g and h are provided in Source Data. (i) Schematic representation of the sphingolipid metabolism pathway, adapted from Zhang et al., 2013[1]. Cer1P – Ceramide-1-phosphate; S1P – Sphingosine-1-phosphate, SM – Sphingomyelin; GlcCer – Glucosylceramide.

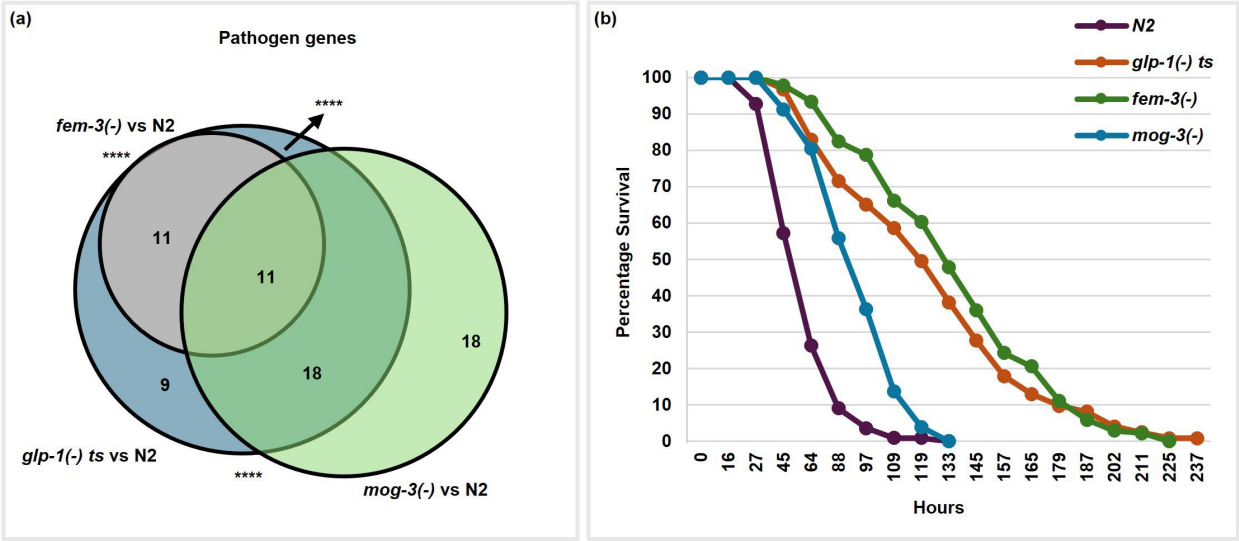

Supplementary Fig. 6: Sterile mutants are less susceptible to PA14 infection. (a) Venn diagram showing the overlaps between the upregulated pathogen response genes in *glp-1(e2144), fem-3(e1996),* and *mog-3(q74)*. The detailed lists of genes and overlaps are shown in Supplementary Data 2. Fisher's exact test was used to assess the significance of overlaps in panel b, c and d. **** indicates p-value < 0.0001. (b). Survival curves showing the lifespans of N2, *glp-1(e2144)*, *fem-3(e1996)* and *mog-3(q74)* worms upon *Pseudomonas aeruginosa (PA14)* infection in a slow-killing assay at 25ºC. Worms were exposed to PA14 starting at day 4 of adulthood to avoid death of wild-type N2 worms from "bagging" (progeny hatching inside the uterus). All three sterile strains showed better survival upon PA14 infection. In panel b, two biological replicates were analyzed for each genotype. Detailed mean lifespan values, the number of worms analyzed per replicate, and corresponding statistical analyses are provided in Source Data.

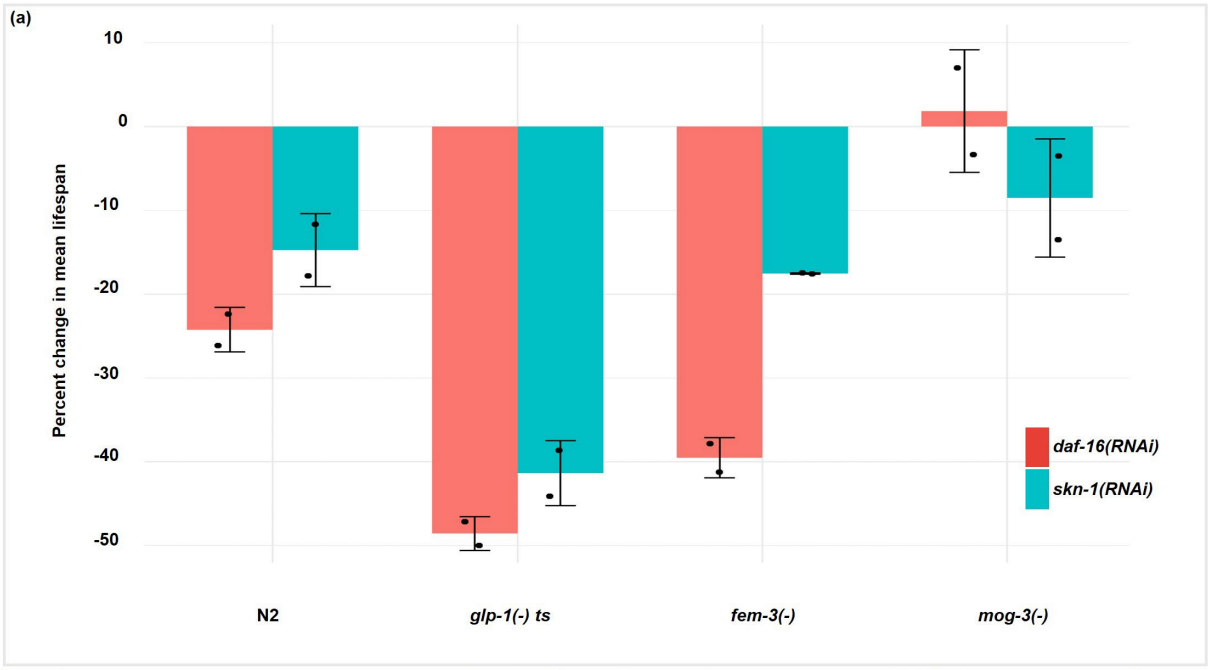
(a)
10
0
-10
-20
-30
-40
-50
Percent change in mean lifespan
daf-16(RNAi)
skn-1(RNAi)
N2
glp-1(-) ts
fem-3(-)
mog-3(-)

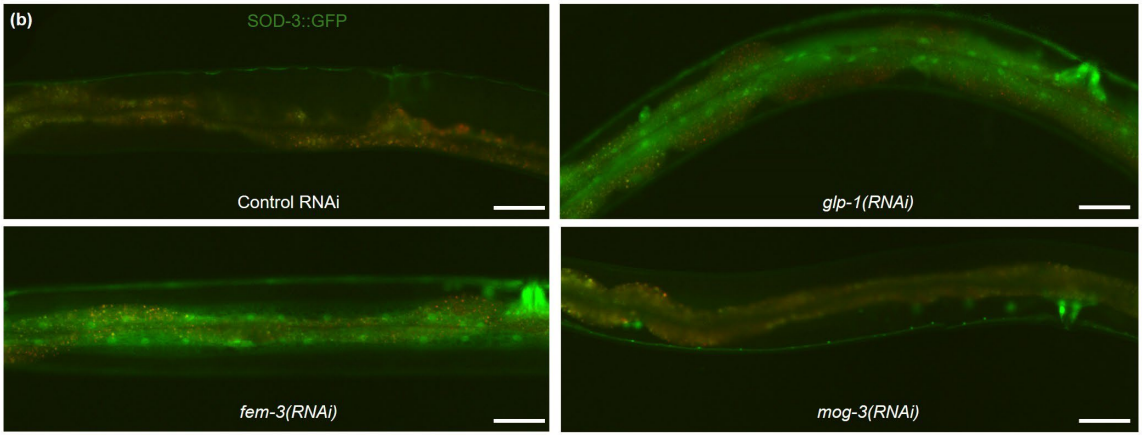
(b)
SOD-3::GFP
Control RNAi
glp-1(RNAi)
fem-3(RNAi)
mog-3(RNAi)

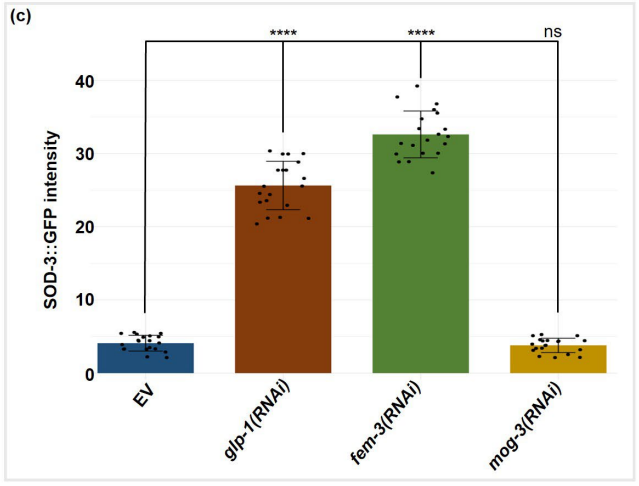
(c)
****
****
ns
40
30
20
10
0
SOD-3::GFP intensity
EV
glp-1(RNAi)
fem-3(RNAi)
mog-3(RNAi)

Supplementary Fig. 7: The lifespans of different sterile mutants are dependent on distinct genetic pathways. (a) Percent change in mean lifespans of N2, *glp-1(e2144)*, *fem-3(e1996)* and *mog-3(q74)* worms upon RNAi depletion of *daf-16* and *skn-1* (survival curves shown in Figure 4a-d). The percentage change in mean lifespan shown here represents the average of two replicates. Detailed mean lifespan values, the number of worms analyzed in each replicate, and statistical analysis for panel a are provided in Source Data. These data correspond to the experiments shown in Fig. 4a and 4b. (b, c) Representative images (b) and quantification (c) showed that nuclear localization of SOD-3::GFP is elevated in *glp-1(RNAi)* and *fem-3(RNAi)* worms but not in *mog-3(RNAi)* worms. The Y-axis represents the mean SOD-3::GFP intensity from two biological replicates per genotype, with at least 10 worms per replicate and 20 worms total per genotype. In panel c, the p-values for comparisons with empty vector (EV) RNAi control are 4.02×10^{-19} for *glp-1(RNAi)*, 2.36×10^{-22} for *fem-3(RNAi)*, and 0.361 for *mog-3(RNAi)*, respectively. In panels c unpaired two-tailed Welch's t-tests were used to perform one-way comparisons of each genotype to EV RNAi control. No correction for multiple comparisons was applied. Statistical significance was set at $p < 0.05$. *p*-values for the tests are indicated as ****p < 0.0001, and ns for not significant. Error bars represent standard deviations. Scale bars in (b), 100 μm.

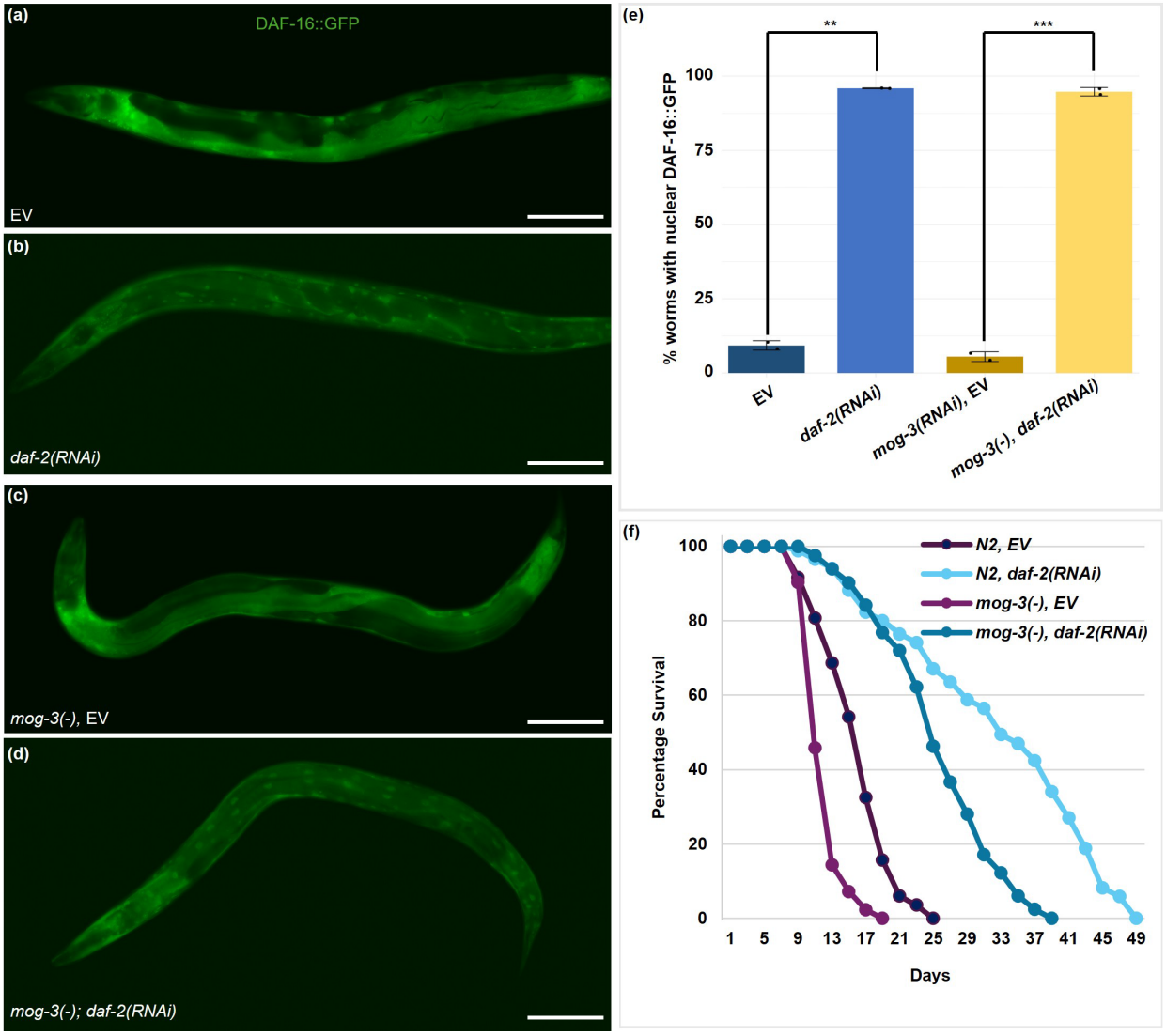

Supplementary Fig. 8: Ectopic nuclear localization of DAF-16 extends the lifespan of mog-3(-) mutants. (a, b, c, d, e) Representative images (a, b, c, d) and quantification (e) showed the nuclear localization of DAF-16::GFP upon *daf-2* RNAi depletion. The Y-axis in (e) depicts the mean percentage of worms exhibiting nuclear GFP localization, derived from analysis of two replicates of each genotype, with a minimum of 50 worms per replicate. Arrowheads mark nuclear DAF-16::GFP. Error bars represent standard deviations. For panel e, the mean percentage of worms exhibiting nuclear DAF-16::GFP localization is shown, based on two biological replicates per genotype, with at least 45 worms per replicate. The total number of worms analyzed per genotype was: 97 (EV), 98 [*daf-2 (RNAi*)], 91 [*mog-3(-),* EV], and 95 [*mog-3(-), daf-2 (RNAi)*]. The p-values for EV vs. *daf-2(RNAi)* and *mog-3(-)*, EV vs. *mog-3(-), daf-2(RNAi)* are 0.0079 and 0.00034, respectively. Unpaired two-tailed Welch's t-tests were used for both pairwise comparisons. No correction for multiple comparisons was applied. Statistical significance was set at $p < 0.05$. p-values for the tests are indicated as $^{**}p < 0.01$, $^{***}p < 0.001$. Scale bars in panels a-d, 100 µm. (f) Survival curves showing the lifespans of wild-type N2, and *mog-3(q74)*

worms upon *daf-2* RNAi. *daf-2* RNAi depletion extends the lifespan of *mog-3(-)* mutants. In panel f, two biological replicates were analyzed for each genotype. Detailed mean lifespan values, the number of worms analyzed per replicate, and corresponding statistical analyses are provided in Source Data.

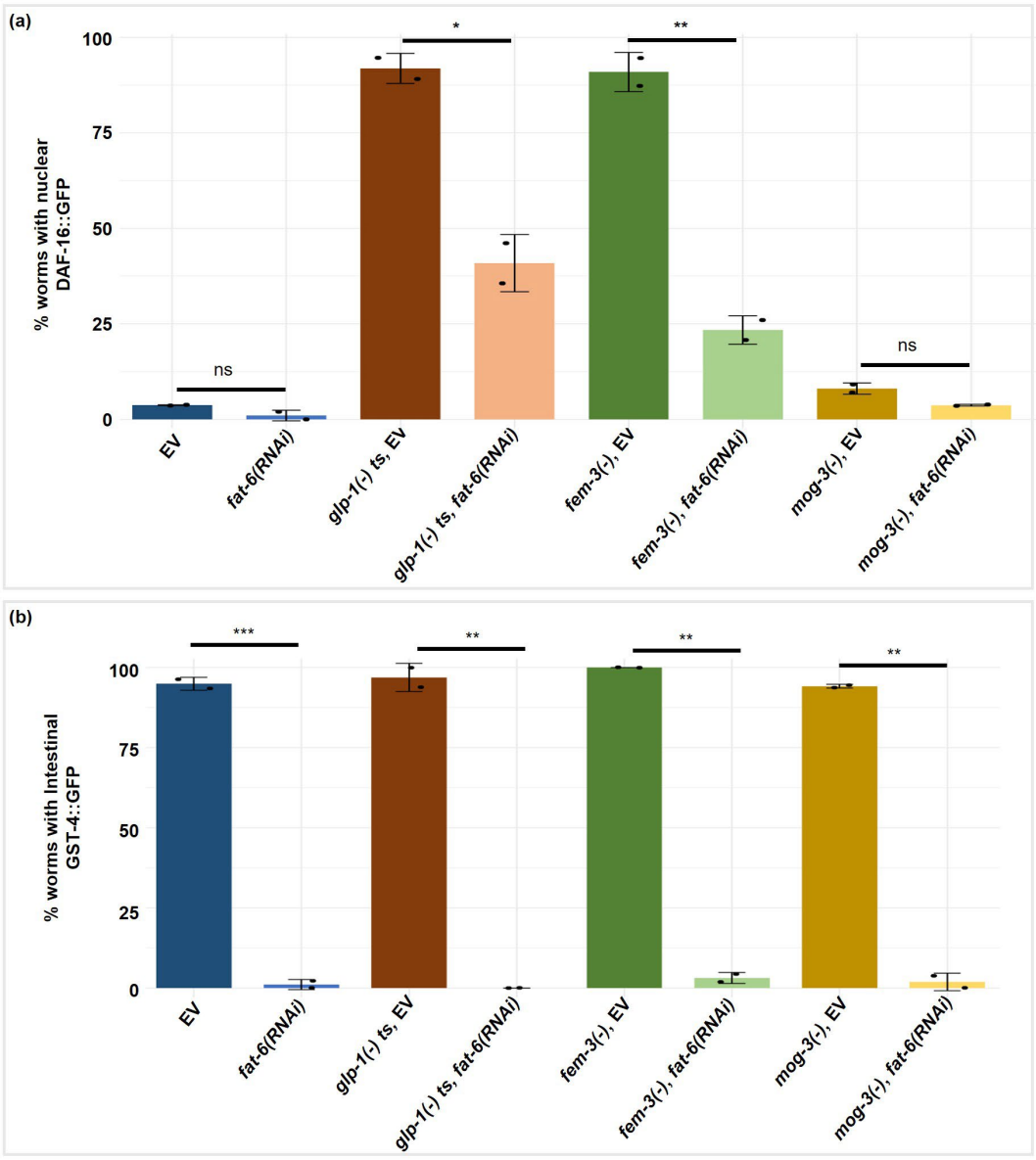

Supplementary Fig. 9: DAF-16::GFP and GST-4::GFP activation are differentially dependent on available fat. **(**a) Percent worms with nuclear DAF-16::GFP in the indicated genotypes. RNAi depletion of *fat-6* partially attenuated DAF-16::GFP nuclear localization. For panel a, the mean percentage of worms exhibiting nuclear DAF-16::GFP localization is shown, based on two biological replicates per genotype, with at least 50 worms per replicate. The total number of worms analyzed per genotype was: 108 [N2, EV], 112 [N2, *fat-6 (RNAi)*], 111 [*glp-1(-),* EV], 111 [*glp-1(-), fat-6 (RNAi)*], 108 [*fem-3(-),* EV], 103 [*fem-3(-), fat-6 (RNAi)*], 112 [*mog-3(-),* EV], and 109 [*mog-3(-), fat-6 (RNAi)*]. In panel a, p-values for comparisons between EV control RNAi and *fat-6(RNAi)* in WT, *glp-1(-) ts*, *fem-3(-)*, and *mog-3(-)* mutants are 0.218, 0.0292, 0.0063, and 0.140, respectively. (b) Percent worms with intestinal GST-4::GFP in the indicated genotypes. RNAi depletion of *fat-6* completely abolished intestinal GST-4::GFP expression. For panel b, the mean percentage of worms exhibiting intestinal GST-4::GFP localization is shown, based on two biological replicates per genotype, with at least 45 worms per replicate. The total number of worms analyzed per genotype was: 101 [N2, EV], 99 [N2, *fat-6 (RNAi)*], 104 [*glp-1(-),* EV],

96 [(*glp-1(-), fat-6 (RNAi)*], 101 [*fem-3(-),* EV], 97 [*fem-3(-), fat-6 (RNAi)*], 103 [*mog-3(-),* EV], and 97 [*mog-3(-), fat-6 (RNAi)*]. In panel b, the p-values for comparisons between EV control RNAi and *fat-6(RNAi)* in WT, *glp-1(-) ts*, *fem-3(-)*, and *mog-3(-)* mutants are 0.00056, 0.0057, 0.0078, and 0.0099, respectively. These experiments were performed at 25°C. In panels a and b, unpaired two-tailed Welch's t-tests were used for all pairwise comparisons. No correction for multiple comparisons was applied. Statistical significance was set at $p < 0.05$. p-values for the tests are indicated as *$p < 0.05$, **$p < 0.01$, ***$p < 0.001$, and ns for not significant. Error bars represent standard deviations.

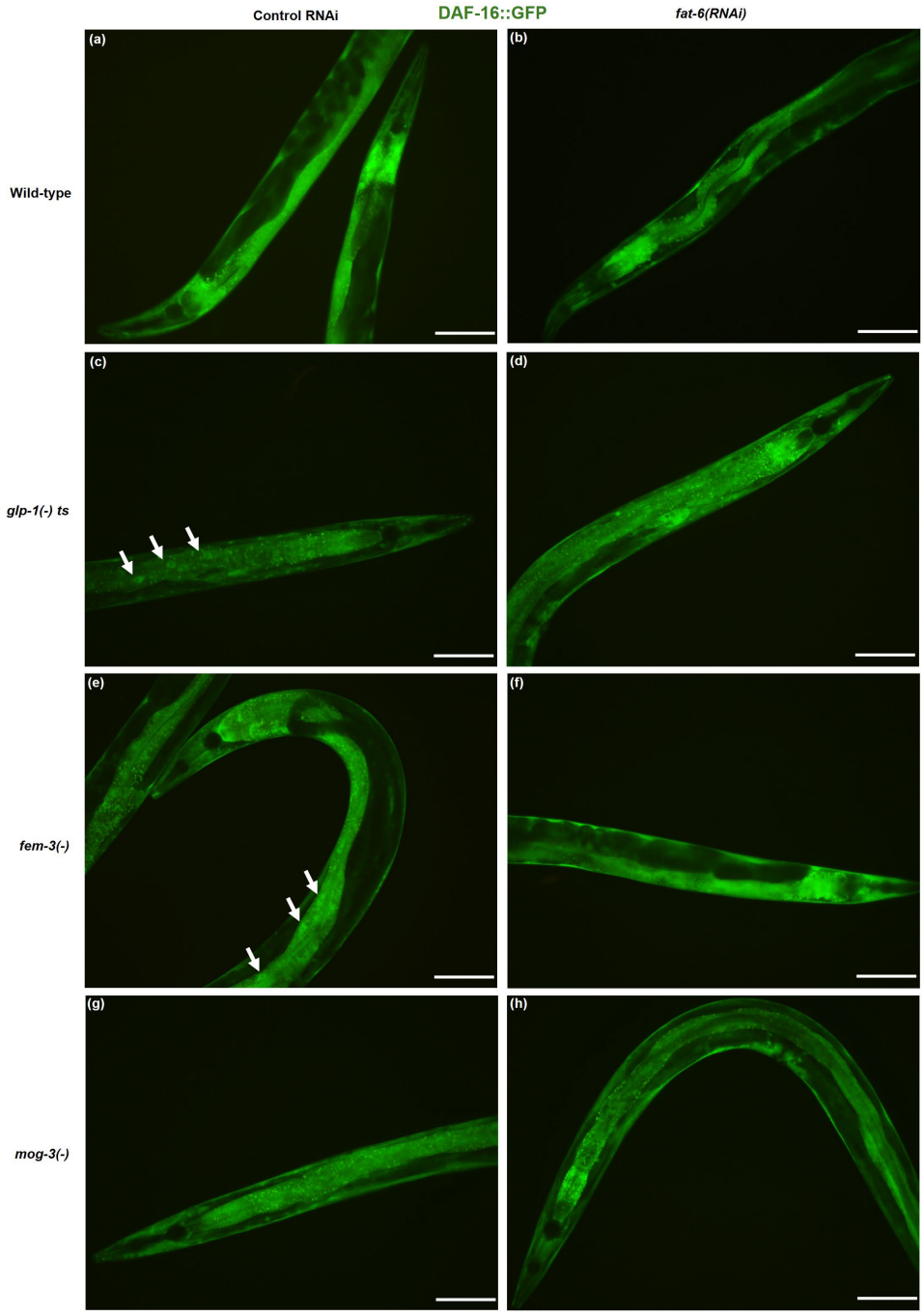

Supplementary Fig. 10: DAF-16 nuclear localization is partially dependent on available fat. (a, c, e, g) The expression of DAF-16::GFP in wild-type (a), *glp-1(e2144)* (c), *fem-3(e1996)* (e) and *mog-3(q74)* (g) worms. Arrowheads show nuclear GFP in *glp-1(e2144)* and *fem-3(e1996)* worms. (b, d, f, h) The expression of DAF-16::GFP in wild-type (**b**), *glp-1(e2144)* (**d**), *fem-3(e1996)* (**f**) and *mog-3(q74)* (**h**) worms upon RNAi depletion of *fat-6.* RNAi depletion of *fat-6* partially rescued the nuclear GFP phenotype (only worms with non-nuclear GFP are shown here). These experiments were performed at 25°C. Scale bars in (a) – (h), 100 µm.

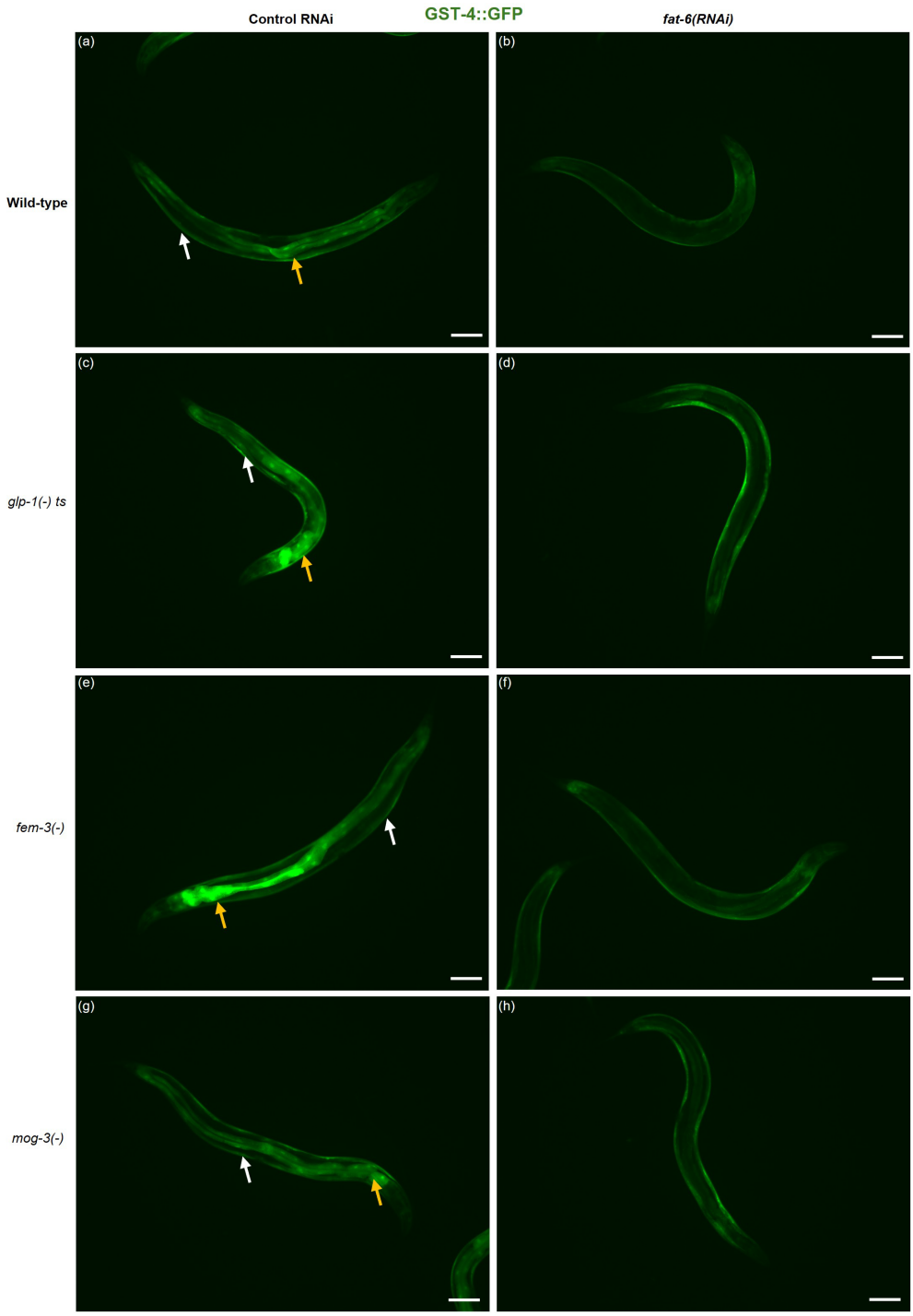

Supplementary Fig. 11: Intestinal SKN-1 activation is completely dependent on available fat. (a, c, e, g) The expression of GST-4::GFP in wild-type (a), *glp-1(e2144)* (c), *fem-3(e1996)* (e) and *mog-3(q74)* (g) worms. White and yellow arrows show hypodermal and intestinal GFP expression, respectively. GST-4::GFP is preferentially activated in the intestines of sterile worms. (b, d, f, h) The expression of GST-4::GFP in wild-type (b), *glp-1(e2144)* (d), *fem-3(e1996)* (f) and *mog-3(q74)* (h) worms upon *fat-6* RNAi. RNAi depletion of *fat-6* specifically deactivated intestinal GST-4::GFP expression. These experiments were performed at 25°C. Scale bars in (a) – (h), 100 µm.

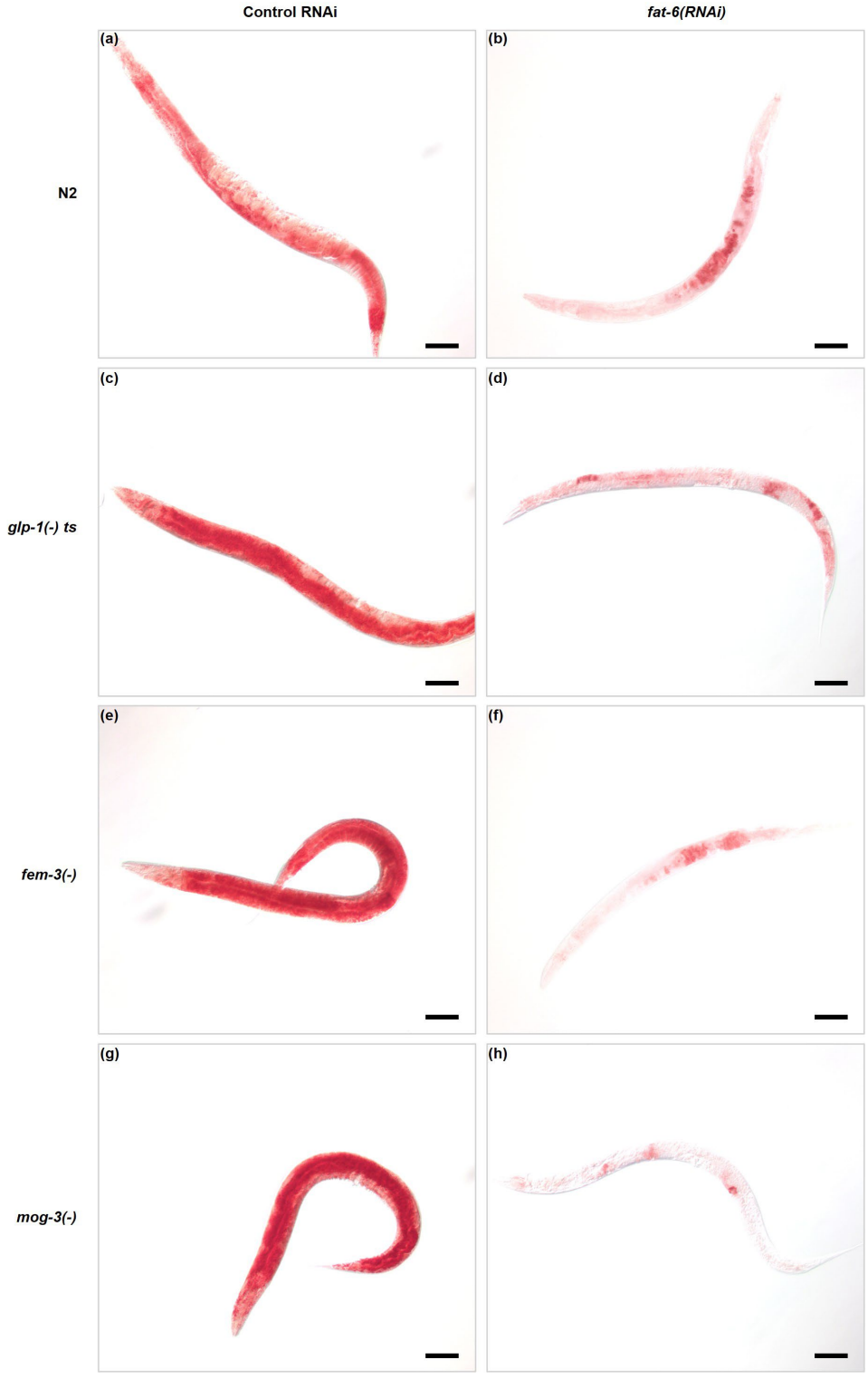

Supplementary Fig. 12: *fat-6* depletion markedly diminishes fat accumulation in all three sterile mutants. Representative images display ORO-stained N2, *glp-1(e2144)*, *fem-3(e1996)*, and *mog-3(q74)* worms treated with an empty vector (EV) control (a, c, e, g) and *fat-6* RNAi (b, d, f, h), respectively. Scale bars in (a) – (h), 100 µm.

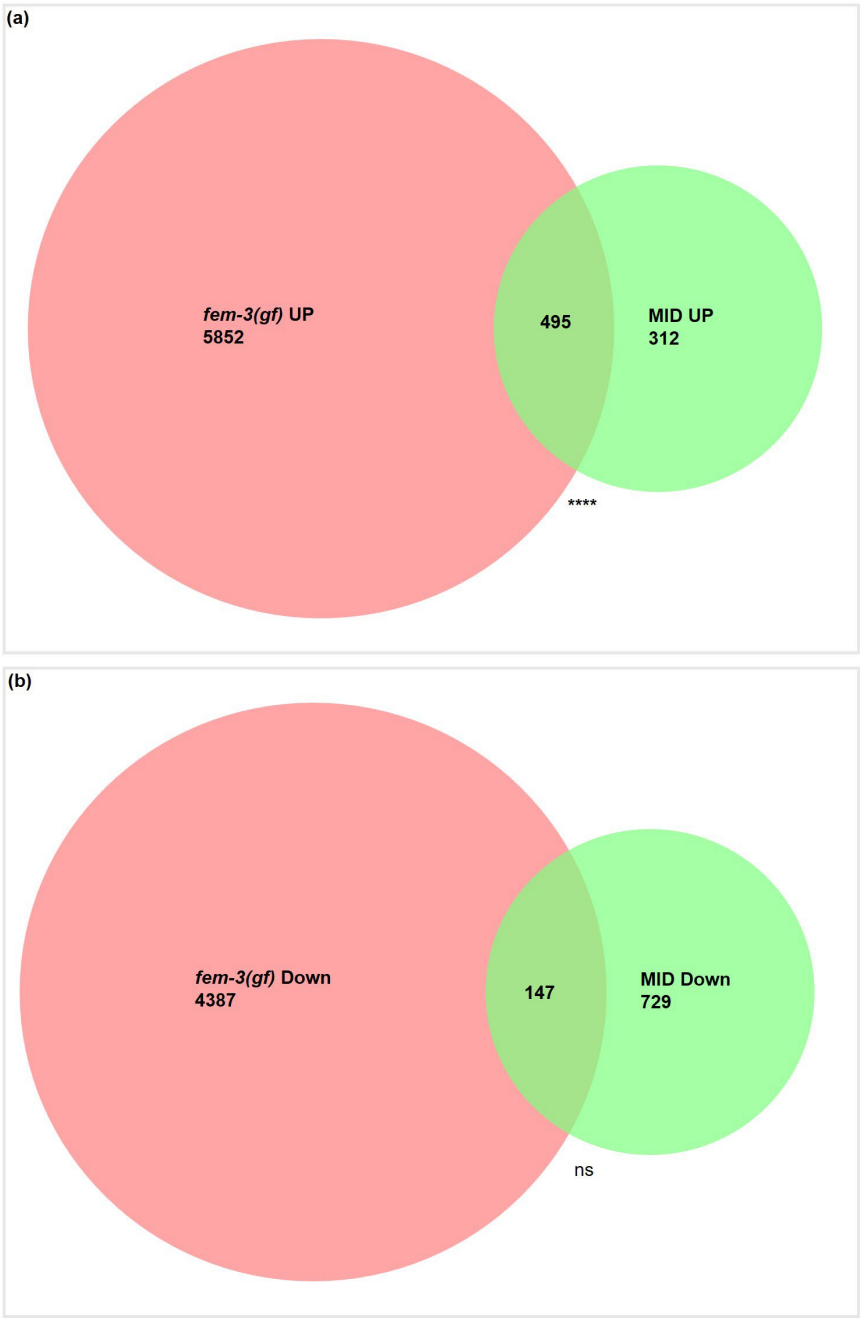

Supplementary Fig. 13: MOG worms exhibit a mating/male-induced demise (MID)-like phenotype. (a, b) Venn diagrams showed the significant overlaps between the upregulated genes in *fem-3(q20)* gain-of-function and genes upregulated in mated worms (a) and downregulated genes in *fem-3(q20)* gain-of-function and genes downregulated in mated worms[2]. A detailed list of genes is provided in Supplementary Data 2. Fisher's exact test was used to assess the significance of overlaps. **** indicates p-value < 0.0001; ns – not significant.

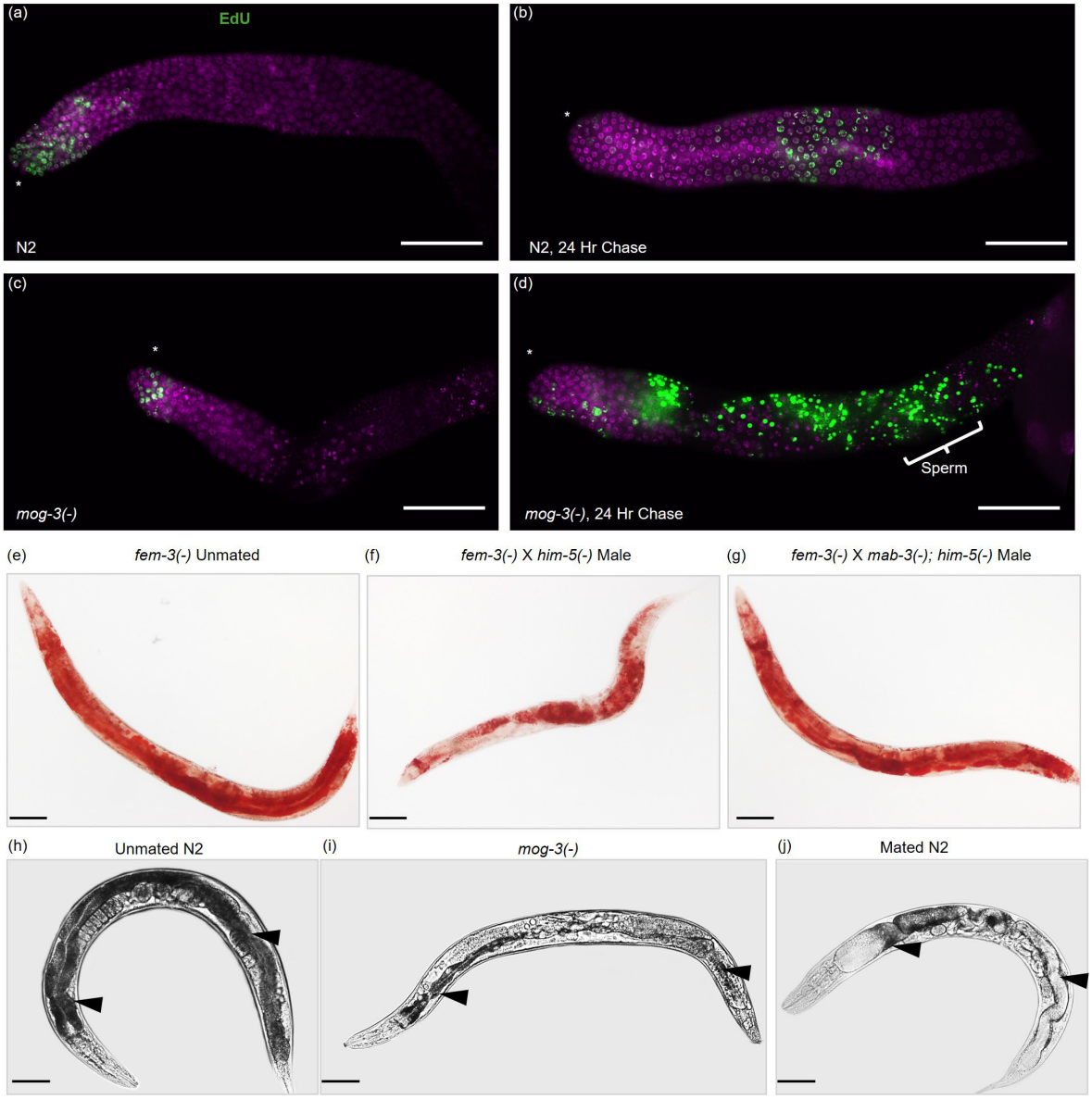

Supplementary Fig. 14: Increased EdU retention and late-onset intestinal decline in *mog-3(-)* mutants lacking early fat loss. (a-d) Representative EdU (5-ethynyl-2′-deoxyuridine) staining images of dissected gonads from N2 (a), N2 after a 24-hour chase (b), *mog-3(q74)* (c), and *mog-3(q74)* after a 24-hour chase (d). Asterisks (*) indicate the distal germline. (e-g) Oil Red O (ORO) staining of day 7 adult (e) unmated feminized *fem-3(-)* worms, (f) *fem-3(1996)* worms mated with wild-type *him-5(e1490)* males, and (g) *fem-3(-)* worms mated with sperm transfer–defective *mab-3(mu15); him-5(e1490)* males. (h-j) Differential Interference Contrast (DIC) images showing intestinal morphology in 7-day-old adult worms: (h) unmated N2, (i) mated N2, and (j) *mog-3(e1490)*.

Supplementary Methods

Lipid enrichment enalysis and visualization

To assess lipid class enrichment across different germline mutants (Fig. 2e), we performed Fisher's exact test using R (v4.3.0). For each lipid class, odds ratios (OR) and p-values were calculated by comparing the number of differentially regulated lipids within each class to the total number detected (n = 1224). Results were visualized as bar plots with significance annotations using ggplot2. For an integrated view of lipid enrichment patterns, enrichment scores and associated p-values for up- and downregulated lipids across mutants were compiled and a bubble plot was generated using ggplot2, where bubble size reflects the enrichment score and color indicates the $-\log_{10}$-transformed p-value.

Heatmap generation

Z-score normalized heatmaps were generated in R (v4.3.0) using the ComplexHeatmap and circlize packages to visualize differential expression patterns of sphingolipid metabolism genes across genotypes. Heatmaps were constructed for all detected sphingolipid metabolism genes (Supplementary Fig. 5g) and for those significantly altered in at least one genotype (Supplementary Fig. 5h). Log_2 fold change ($\log_2$FC) values from DESeq2 analysis were standardized on a per-gene basis (row-wise z-score). Gene-wise clustering was performed using K-means clustering with k = 6, while genotype-wise (column) clustering was performed using hierarchical clustering based on 1 – Pearson correlation and average linkage.

Supplementary References

1. Zhang, Y. *et al.* Comparative genomics and functional study of lipid metabolic genes in Caenorhabditis elegans. *BMC Genomics* 14, (2013).

2. Booth, L. N. *et al.* Males induce premature demise of the opposite sex by multifaceted strategies. *Nature Aging 2022 2:9* 2, 809–823 (2022).